

SPORADICALLY TORQUED ACCRETION DISKS AROUND BLACK HOLES

DAVID GAROFALO¹ AND CHRISTOPHER S. REYNOLDS²

Received 2004 July 9; accepted 2005 January 14

ABSTRACT

The assumption that black hole accretion disks possess an untorqued inner boundary, the so-called zero-torque boundary condition, has been employed by models of black hole disks for many years. However, recent theoretical and observational work suggests that magnetic forces may appreciably torque the inner disk. This raises the question of the effect that a time-changing magnetic torque may have on the evolution of such a disk. In particular, we explore the suggestion that the “deep minimum state” of the Seyfert galaxy MCG –6-30-15 can be identified as a sporadic inner disk torquing event. This suggestion is motivated by detailed analyses of changes in the profile of the broad fluorescence iron line in *XMM-Newton* spectra. We find that the response of such a disk to a torquing event has two phases: an initial damming of the accretion flow together with a partial draining of the disk interior to the torque location, followed by a replenishment of the inner disk as the system achieves a new (torqued) steady state. If the deep minimum state of MCG –6-30-15 is indeed due to a sporadic torquing event, we show that the fraction of the dissipated energy going into X-rays must be smaller in the torqued state. We propose one such scenario in which Compton cooling of the disk corona by “returning radiation” accompanying a central torquing event suppresses the 0.5–10 keV X-ray flux coming from all but the innermost regions of the disk.

Subject headings: accretion, accretion disks — black hole physics — galaxies: active — galaxies: individual (MCG –6-30-15) — MHD — X-rays: galaxies

1. INTRODUCTION

There is direct evidence that active galactic nuclei (AGNs) are powered by disk accretion onto supermassive black holes. For example, the central regions of the giant elliptical galaxy M87 were spatially resolved by the *Hubble Space Telescope* sufficiently to actually see a ~ 100 pc scale disk of ionized gas in orbit about an unseen mass of $3 \times 10^9 M_{\odot}$, presumed to be a supermassive black hole (Ford et al. 1994; Harms et al. 1994). The fact that this gas disk is approximately normal to the famous relativistic jet displayed by this object is circumstantial evidence that it is, indeed, the outer regions of the accretion disk that power this AGN. In another important case, radio observations of megamasers in the spiral galaxy NGC 4258 (M106) reveal an almost perfectly Keplerian ~ 0.5 pc gas disk orbiting a compact object with mass $3.5 \times 10^7 M_{\odot}$ (Miyoshi et al. 1995; Greenhill et al. 1995).

Even before the observational evidence for black hole accretion disks became compelling, the basic theory of such disks had been extensively developed. Building on the nonrelativistic theory of Shakura & Sunyaev (1973), Novikov & Thorne (1973) and Page & Thorne (1974) developed the “standard” model of a geometrically thin, radiatively efficient, steady state, viscous accretion disk around an isolated Kerr black hole. In addition to the assumptions already listed, it is assumed that the viscous torque operating within the disk becomes zero at the radius of marginal stability, $r = r_{\text{ms}}$. Physically, this was justified by assuming that the accretion flow would pass through a sonic point close to $r = r_{\text{ms}}$ and hence flow ballistically (i.e., “plunge”) into the black hole.

Even while setting up this boundary condition, Page & Thorne (1974) noted that magnetic fields may allow this zero-torque boundary condition (ZTBC) to be violated. Given the modern viewpoint of accretion disks, that the very “viscosity” driving

accretion is due to magnetohydrodynamic (MHD) turbulence, the idea that the ZTBC can be violated has been revived by recent theoretical work, starting with Gammie (1999) and Krolik (1999a). In independent treatments, these authors show that significant energy and angular momentum can be extracted from matter within the radius of marginal stability via magnetic connections with the main body of the accretion disk. Agol & Krolik (2000) have performed the formal extension of the standard model to include a torque at $r = r_{\text{ms}}$ and show that the extra dissipation associated with this torque produces a very centrally concentrated dissipation profile. As shown by Gammie (1999), Agol & Krolik (2000), and Li (2002), this process can lead to an extraction (and subsequent dissipation) of spin energy and angular momentum from the rotating black hole by the accretion disk. In these cases, the magnetic forces might be capable of placing the innermost part of the flow on negative energy orbits, allowing a Penrose process to be realized (we note that Williams [2004] has also argued for the importance of a nonmagnetic, particle-particle and particle-photon scattering mediated Penrose process). A second mechanism by which the central accretion disk can be torqued is via a direct magnetic connection between the inner accretion disk and the (rotating) event horizon of the black hole. In this case, as long as the angular velocity of the event horizon exceeds that of the inner disk, energy and angular momentum of the spinning black hole can be extracted via the Blandford-Znajek mechanism (Blandford & Znajek 1977). We note that field lines that directly connect the rotating event horizon with the body of the accretion disk through the plunging region *are* seen in recent general relativistic MHD simulations of black hole accretion (e.g., Hirose et al. 2004).

Interest in these torqued relativistic disks has received a boost from recent X-ray observations. The X-ray spectra of many AGNs (and, indeed, Galactic black hole candidates) reveal the signatures of “X-ray reflection” from optically thick matter. In some cases, examination of these features allows us to detect strong Doppler and gravitational shifts indicative of circular motion close to a black hole (Fabian et al. 1989, 2000; Tanaka et al.

¹ Department of Physics, University of Maryland, College Park, MD 20742.

² Department of Astronomy, University of Maryland, College Park, MD 20742.

1995; Reynolds & Nowak 2003). In these cases, the observed range of Doppler and gravitational shifts can be used to map the X-ray emission/irradiation across the surface of the accretion disk. The *XMM-Newton* satellite is particularly well suited to the study of these features because of its combination of good spectral resolution and high throughput. Using *XMM-Newton*, Wilms et al. (2001) and Reynolds et al. (2004) studied the Seyfert 1 galaxy MCG –6-30-15 in its peculiar “deep minimum state” first discovered by *ASCA* (Iwasawa et al. 1996). Confirming the principal result of Iwasawa et al. (1996), the X-ray reflection features were found to be extremely broad. The degree of gravitational redshifting required the majority of the X-ray emission to emerge within a radius of $r \sim 2GM/c^2$ from a near-extremal Kerr black hole (i.e., a black hole with a spin parameter of $a = 0.998$). As explicitly shown in Reynolds et al. (2004), it is very problematic to explain these data within the framework of the standard accretion disk model. Fabian & Vaughan (2003) and Miniutti & Fabian (2004) suggest that gravitational focusing of the primary continuum X-rays might produce such a centrally concentrated emissivity profile. Alternatively, Reynolds et al. (2004) have shown that a torqued disk can readily explain the deep minimum spectrum, provided that the source is assumed to be in a torque-dominated state (or, in the terminology of Agol & Krolik [2000], an “infinite-efficiency” state) whereby the power associated with the innermost torque is instantaneously dominating the accretion power. In other words, the X-ray data suggest that during this deep minimum state of MCG –6-30-15 the power derived from the black hole spin greatly exceeds that derived from accretion.

Of course, this state of affairs cannot last forever, or else the central black hole in MCG –6-30-15 would spin down to a point where it could no longer provide this power. At some point in its history, the system must be in an accretion-dominated phase in which the black hole is spun up. However, even in its spin-dominated state, the spin-down timescale of the central black hole is of the order of 10^8 yr or more. Thus, we could envisage a situation in which the system shines via a quasi-steady state, spin-dominated accretion disk. There are hints, though, that accretion disks may switch between spin-dominated and accretion-dominated on much shorter timescales. In its normal spectral state, the X-ray reflection features in MCG –6-30-15 are much less centrally concentrated than in the deep minimum state, suggesting that the normal state might be accretion dominated. It is also important to note that this system can switch between its normal state and the deep minimum state in as little as 5–10 ks (Iwasawa et al. 1996), which corresponds to only a few dynamical timescales of the inner accretion disk. Thus, it is of interest to consider the physics of an accretion disk that undergoes a rapid torquing event. That is the prime motivation for this paper.

In § 2 we begin our study of sporadically torqued accretion disks by investigating an analytic solution for a torqued Newtonian disk. In § 3, we generalize to the fully relativistic equations and obtain numerical solutions. In § 4, we relate our results to the observed properties of the “deep minimum state” of MCG –6-30-15 and consequently discuss the effect that a torquing event may have on the physics of the X-ray-emitting disk corona. In particular, we suggest that the enhanced returning radiation associated with a torquing event might suppress 0.5–10 keV coronal emission in all but the inner portion of the disk. Section 5 summarizes our main conclusions.

2. AN ANALYTIC “TOY” MODEL OF A TORQUED DISK

We begin our investigation of sporadically torqued disks via the study of a simple case that lends itself to a straightforward

analytic solution. We construct a model of a radiatively efficient accretion disk following the usual approach of Pringle (1981). We assume that the accretion disk is axisymmetric, geometrically thin, and in Keplerian motion about a point mass M . Using a cylindrical polar coordinate system (r, z, ϕ) with the axis passing through the central mass normal to the disk plane, we denote the surface density of the disk by $\Sigma(r, t)$, the angular velocity of the disk about M as $\Omega(r)$, and the radial velocity of the disk material as $v_r(r, t)$. The equations that determine the structure of the thin disk assuming radiative efficiency are mass and angular momentum conservation,

$$r \frac{\partial \Sigma}{\partial t} + \frac{\partial (rv_r \Sigma)}{\partial r} = 0, \quad (1)$$

$$r \frac{\partial (\Sigma r^2 \Omega)}{\partial t} + \frac{\partial (r \Sigma v_r r^2 \Omega)}{\partial r} = \frac{1}{2\pi} \frac{\partial G}{\partial r}, \quad (2)$$

respectively, where $G(r, t)$ is the torque exerted by the disk *outside* radius r on the disk *inside* that radius.

In standard disk models, the torque G is the integrated value of the only stress tensor component ($S_{r\phi}$) that survives the condition of axisymmetry and geometric thinness. From Krolik (1999b, p. 139) we have

$$G = \int r S_{r\phi} dz \int r d\phi = 2\pi r^3 \nu \Sigma \frac{\partial \Omega}{\partial r}, \quad (3)$$

where we have introduced an “effective kinematic viscosity,” ν . To generalize these models to the case of an externally imposed torque, we set

$$G = 2\pi r^3 \nu \Sigma \frac{\partial \Omega}{\partial r} + G_T. \quad (4)$$

Combining equations (1), (2), and (4) and specializing to a Keplerian rotation curve, we get the usual diffusion equation for surface density modified for the effects of the external torque,

$$\frac{\partial \Sigma}{\partial t} = \frac{3}{r} \frac{\partial}{\partial r} \left[r^{1/2} \frac{\partial (\nu \Sigma r^{1/2})}{\partial r} \right] - \frac{1}{r\pi(GM)^{1/2}} \frac{\partial}{\partial r} \left(r^{1/2} \frac{\partial G_T}{\partial r} \right). \quad (5)$$

For the rest of this paper, we work in units where $GM = 1$. Changing variables to $x = r^{1/2}$ and $\psi = \nu \Sigma x$ and assuming that ν has no explicit time dependence, we get

$$\frac{\partial \psi}{\partial t} = \frac{3\nu}{4x^2} \frac{\partial^2}{\partial x^2} \left(\psi - \frac{G_T}{3\pi} \right). \quad (6)$$

We now consider a particular torquing event. Suppose that the disk suffers no external torques for the period $t < 0$. Then, at $t = 0$, we engage an external torque (possibly resulting from a magnetic connection to the plunging region or spinning event horizon) that deposits angular momentum into a narrow annulus at $r = r_0$. If the rate at which angular momentum is being deposited is β , we have

$$\frac{\partial G_T}{\partial r} = \beta \delta(r - r_0) \Theta(t), \quad (7)$$

giving

$$G_T(r, t) = \beta \Theta(r - r_0) \Theta(t), \quad (8)$$

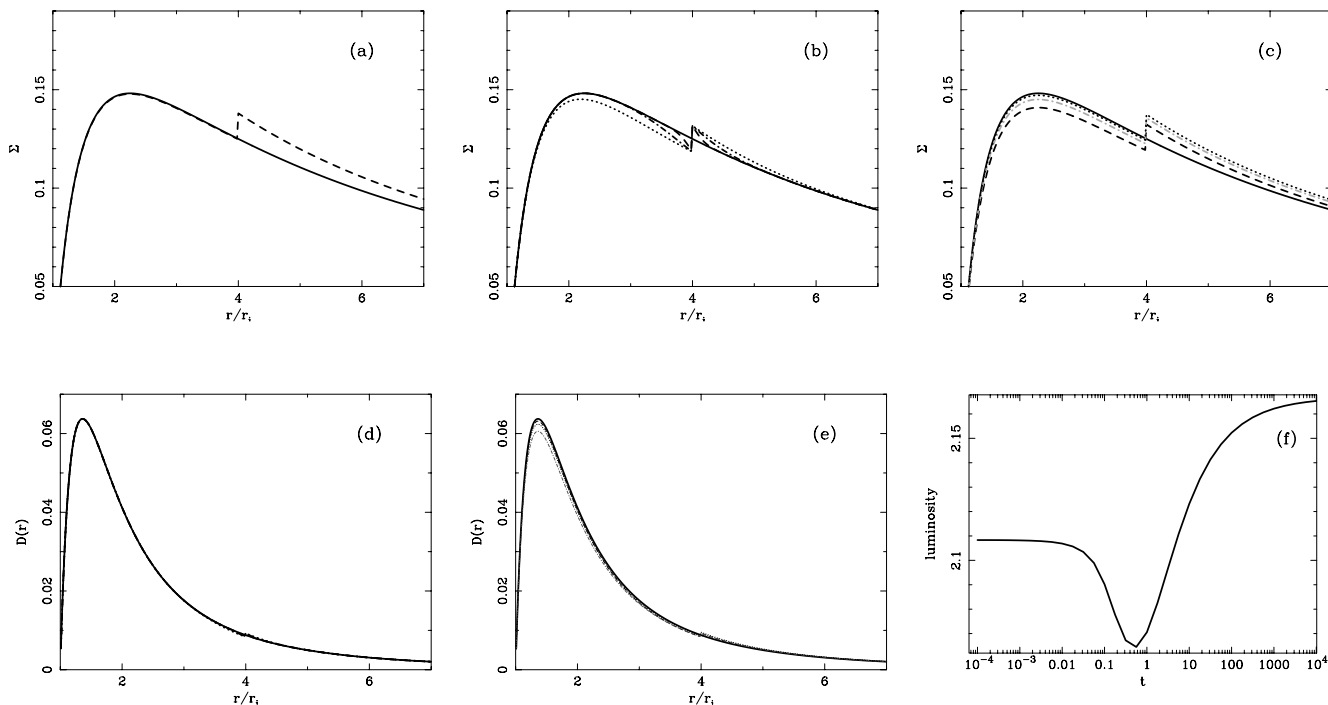


FIG. 1.—Evolution of our “toy” model disk with a torque acting at $r = 4$. (a) Initial state of the surface density profile for the nontorqued disk (solid line) and the resulting torqued steady state (dashed line). (b) Four times in the early evolution of the surface density profile (solid line: $t = 0$, the untorqued steady state; dashed line: $t = 10^{-3}$; dot-dashed line: $t = 10^{-2}$; dotted line: $t = 10^{-1}$; we use units such that $k = 1$, which corresponds to scaling with respect to the viscous timescale of the inner disk). Note how the initial evolution is such that density drops inward of the torque location and increases outward of it because of the “damming” of the accretion flow. (c) Subsequent late evolution toward the torqued steady state (solid line: $t = 0$, or untorqued steady state; dashed line: $t = 1$; dot-dashed line: $t = 10$; dotted line: $t = 100$). (d, e) Dissipation profiles $D(r)$ in the early and late stages, respectively, of the evolution with the type of line and time corresponding to those of (b) and (c). In this case, the effect on $D(r)$ is subtle. (f) Luminosity profile obtained by integrating the dissipation profile over the disk surface. The final steady state torqued luminosity profile is enhanced with respect to the nontorqued steady state profile because of work done by the torque.

where Θ is the Heaviside step function. At this point, we specialize to a particular viscosity law. We set $\nu = kr$ for mathematical convenience, although it will not make qualitative difference. We can now rewrite equation (6) as

$$\frac{\partial \xi}{\partial t} = \frac{3k}{4} \left(\frac{\partial^2 \xi}{\partial x^2} \right) - \frac{\beta}{3\pi} \Theta(x - x_0) \delta(t), \quad (9)$$

where

$$\xi = \psi - \frac{\beta}{3\pi} \Theta(x - x_0) \Theta(t), \quad (10)$$

and the δ -function in time results from the time derivative of the $\Theta(t)$ term.

Suppose that the disk is in the untorqued steady state at $t < 0$. From equation (9), one can easily see that such a steady state is given by

$$\xi_{\text{ss}} = \psi = A(x - x_i) \quad (t < 0), \quad (11)$$

where A is a normalization constant and $r_i \equiv x_i^2$ is the inner edge of the untorqued disk defined as the location where the “viscous” torques vanish. Examination of equation (9) shows that the time-dependent behavior of the torqued disk at times $t > 0$ is given by the simple diffusion equation

$$\frac{\partial \xi}{\partial t} = \frac{3k}{4} \frac{\partial^2 \xi}{\partial x^2}, \quad (12)$$

with an initial condition set by integrating through the δ -function in time, $\xi(x, t = 0) = \xi_{\text{ss}} - \beta \Theta(x - x_0) / 3\pi$. The appropriate bound-

ary condition is $\xi \rightarrow \xi_{\text{ss}}$ as $t \rightarrow \infty$. Standard methods (i.e., separation of variables) give the following solution:

$$\xi(x, t) = \xi_{\text{ss}}(x) + \frac{\beta}{3\pi^2} \int_0^\infty \frac{1}{\lambda} [\sin \lambda x_0 \cos \lambda x - (\cos \lambda x_0 + 1) \sin \lambda x] \exp\left(\frac{-3k\lambda^2 t}{4}\right) d\lambda. \quad (13)$$

With this solution, we can compute the surface density of the disk at any given radius and time. Armed with the surface density, we can then compute all other quantities of interest including the viscous dissipation rate per unit surface area of the disk:

$$D(r) = \frac{\nu \Sigma r^2}{2} \Omega'^2, \quad (14)$$

where $\Omega' = d\Omega/dr$. Plots of the radial dependence of $\Sigma(r)$ and $D(r)$ for various times are shown in Figures 1 and 2. Also shown is the time dependence of the total viscous dissipation obtained by integrating $D(r)$ across the whole disk (i.e., luminosity). We can see that the response of the disk to the onset of an external torque can be separated into two phases. In the first phase, the accretion flow is “dammed” at $r = r_0$ because of the inability of the accretion flow to transport the angular momentum deposited by the external torque. This leads to a buildup of mass (i.e., an increase in the surface density) in the region $r > r_0$. Concurrently, matter in the region $r < r_0$ continues to accrete, thereby partially draining away the surface density. The inevitable result is a growing discontinuity in the surface density at $r = r_0$. The angular momentum transport associated with this discontinuity grows until mass can, once again, flow inward across

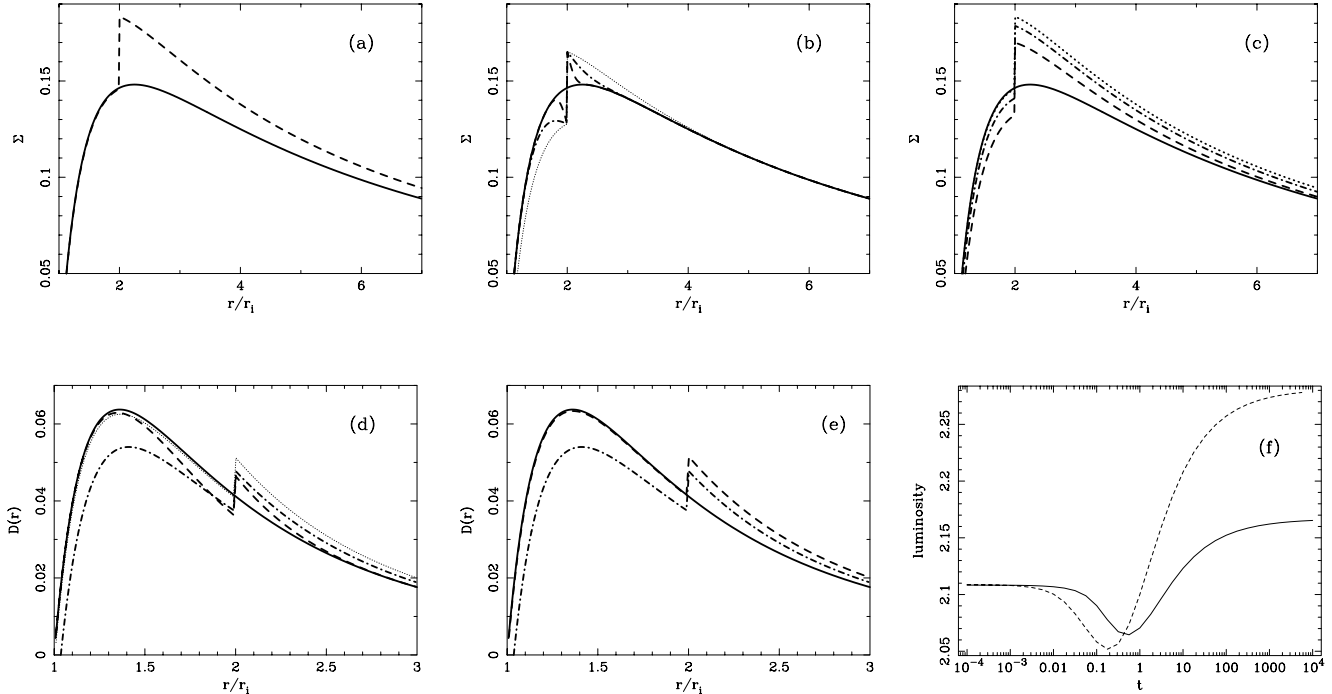


FIG. 2.—Evolution of our “toy” model disk with a torque acting at $r = 2$. (a) Initial state of the surface density profile for the nontorqued disk (solid line) and the resulting torqued steady state (dashed line). (b) Four times in the early evolution of the surface density profile (solid line: $t = 0$, dashed line: $t = 10^{-3}$, dot-dashed line: $t = 10^{-2}$, dotted line: $t = 10^{-1}$). (c) Subsequent late evolution toward the torqued steady state (dashed line: $t = 1$, dot-dashed line: $t = 10$, dotted line: $t = 100$). For reference, the lower solid line shows the untorqued steady state disk. (d, e) Dissipation profiles $D(r)$ in the early and late stages, respectively, of the evolution with the same line type/time arrangement as Fig. 1. In other words, the line types of (b) match those of (d) and those of (c) match those of (e). (f) Luminosity profile obtained by integrating the dissipation profile over the disk surface for both torques at $r = 2$ (dashed line) and $r = 4$ (solid line).

this radius. One then enters the second phase of evolution, whereby the surface density in the region $r < r_0$ is replenished back to its original level while the surface density discontinuity is maintained at approximately a constant level. Eventually, one achieves the torqued steady state solution (e.g., Agol & Krolik 2000). The two sets of figures are for an external torque at $r = 4$ and one closer to the inner edge at $r = 2$. Note how, for a given injection rate of angular momentum, the effect on the disk structure is much more dramatic for smaller radius.

Since our disks are assumed to be radiatively efficient, the instantaneous total luminosity of the accretion disk can be formally decomposed into two components, one due to the decrease in gravitational potential energy of the accreting gas and a second due to the work done by the external torque, i.e.,

$$L = 2 \int 2\pi r D(r) dr = \frac{1}{2} \int \frac{GM\dot{M}}{r^2} dr + \int \Omega \frac{\partial G_T}{\partial r} dr. \quad (15)$$

As can be seen from Figures 1f and 2f, the luminosity dips before climbing up to a new elevated level that includes the work done by the external torque, as well as the accretion energy. The temporary dip in luminosity is due to the damming of the accretion flow in the early evolution of the torquing event.

Now that we have explored a torquing event via the analytical solution of an extremely simplified accretion disk model, we move on to somewhat more realistic models. In the next section, we present a semianalytic analysis of a geometrically thin general relativistic accretion disk.

3. RELATIVISTIC TORQUED ACCRETION DISKS

Relativity produces two complications to the analysis. First, the equations governing the structure of the accretion disk are

rather more complex and drive us to use numerical rather than analytic techniques. Second, the relationship between the emitted and observed fluxes becomes nontrivial, with gravitational light bending, relativistic aberration/beaming, and Doppler/gravitational redshifting all becoming important. We deal with each of these issues in turn.

The time-dependent equations describing the structure of a geometrically thin accretion disk in the $\theta = \pi/2$ plane of a Kerr spacetime are given in Boyer-Lindquist coordinates (t, R, θ, ϕ) by Eardley & Lightman (1975). Taking $\Sigma(R)$ to be the proper surface density of the disk (i.e., the surface density measured by a local observer moving with the fluid), the disk evolution is described by

$$\frac{\partial \Sigma}{\partial t} = \frac{c^{1/2}}{BR} \frac{\partial}{\partial R} \left[\frac{\Gamma}{\partial L^\dagger / \partial R} \frac{\partial}{\partial R} (\mathcal{W} R^2 \mathcal{D}) \right], \quad (16)$$

where

$$\mathcal{B} = 1 + \frac{aM^{1/2}}{R^{3/2}}, \quad (17)$$

$$\mathcal{C} = 1 - \frac{3M}{R} + \frac{2aM^{1/2}}{R^{3/2}}, \quad (18)$$

$$\mathcal{D} = 1 - \frac{2M}{R} + \frac{a^2}{R^2}, \quad (19)$$

$$\Gamma = \frac{\mathcal{B}}{c^{1/2}}, \quad (20)$$

$$L^\dagger = M^{1/2} R^{1/2} \left(1 - \frac{2aM^{3/2}}{R^{3/2}} + \frac{a^2 M^2}{R^2} \right). \quad (21)$$

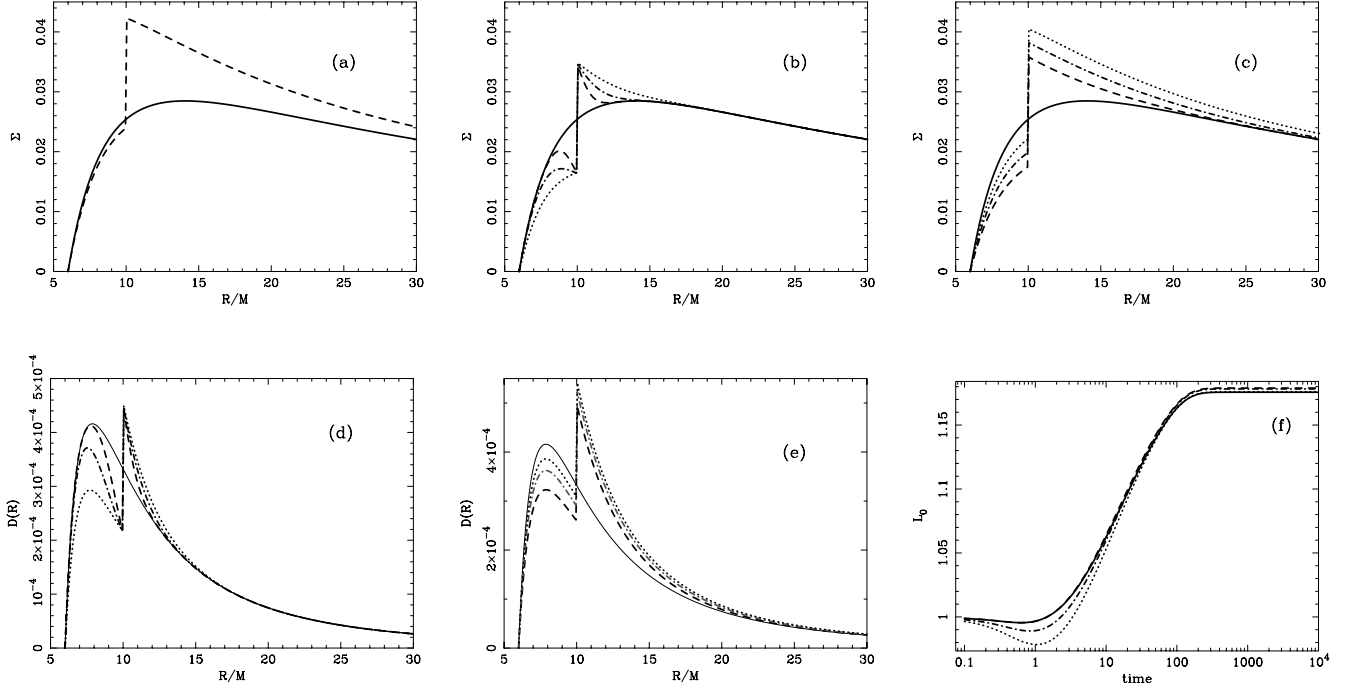


FIG. 3.—Evolution of disk in Schwarzschild spacetime for torque at $R/M = 10$. (a) Surface density profile just after the torquing event begins, as well as when the steady state torqued profile is approached (*dashed line*: $t = 10,000$). (b) Early stages in the evolution of the surface density profile with the solid line being the untorqued steady state profile (*dashed line*: $t = 0.8$, *dot-dashed line*: $t = 2.53$, *dotted line*: $t = 8.0$). (c) Untorqued steady state profile (*solid line*), as well as the late-time evolution of the torqued profile (*dashed line*: $t = 25$, *dot-dashed line*: $t = 80$, *dotted line*: $t = 253$). (d) Early evolution of the dissipation function with lines and times corresponding to those of (b). The qualitative feature is again a drop inward of the torque location and an increase outward. (e) Late-time evolution of dissipation function with lines and times analogous to those of (c), while (f) shows the observed luminosity starting at an untorqued steady state with $t = 0$. The observed luminosity is determined for angles of 10° (*solid line*), 30° (*dashed line*), 60° (*dot-dashed line*), and 80° (*dotted line*). Although the magnitude of the observed luminosity is not the same in the untorqued steady state for all angles, we have normalized them in order to see the change with respect to the untorqued state. Note the presence of a drop in the luminosity as the angle of inclination decreases.

Here a is the dimensionless spin parameter of the black hole (denoted as a_* by Eardley & Lightman 1975) and L^\dagger is the specific angular momentum of the fluid for prograde orbits. The local $r\phi$ shear in this flow is $\sigma = -3\Omega\mathcal{C}^{-1}\mathcal{D}$, where $\Omega = (M/r^3)^{1/2}$. Thus, guided by the nonrelativistic prescription, we set the vertically integrated $r\phi$ component of the stress tensor in the absence of an external torque to be

$$\mathcal{W} = -\nu\sigma\Sigma = \frac{3}{2}\nu\Sigma\frac{M^{1/2}}{R^{3/2}}\frac{\mathcal{D}}{\mathcal{C}}, \quad (22)$$

where ν is the same effective viscosity that appeared in the nonrelativistic expressions. Noting that the total *torque* is given by $G = 2\pi WR^2\mathcal{D}$, we see that the appropriate relativistic diffusion equation describing a sporadically torqued disk (i.e., the counterpart to eq. [6]) is

$$\frac{\partial\Sigma}{\partial t} = \frac{\mathcal{C}^{1/2}}{2\pi BR} \frac{\partial}{\partial R} \left[\frac{\Gamma}{\partial L^\dagger / \partial R} \frac{\partial}{\partial R} \left(\frac{3\mathcal{D}^2}{2\mathcal{C}} \nu\Sigma M^{1/2} R^{1/2} - \frac{G_T}{2\pi} \right) \right]. \quad (23)$$

It is straightforward to verify that equation (23) reduces to equation (5) in the nonrelativistic limit [i.e., $\mathcal{B}, \mathcal{C}, \mathcal{D} \rightarrow 1; L^\dagger \rightarrow (MR)^{1/2}$]. The complications introduced by the relativistic factors render this equation intractable to elementary solution methods. Thus, we use a simple explicit scheme to numerically solve this diffusion equation following the treatment of Press

et al. (1992). Figures 3 and 4 show the temporal behavior of an accretion disk around Schwarzschild ($a = 0$) and near-maximal Kerr ($a = 0.998$) black holes, respectively. To facilitate comparison with the nonrelativistic case, we have chosen the same viscosity law, $\nu = kR$ (i.e., ν scales with the radial Boyer-Lindquist coordinate and not the proper distance). As in the Newtonian case, this prescription does not change the results qualitatively. Note that the behavior is similar to that found in the nonrelativistic model. The two phases of evolution, the damping phase and the replenishing phase, are reproduced. The differences do not come from the dynamics but from the boundary conditions that are determined by the equilibrium conditions for circular geodesics. The presence of an innermost stable circular orbit for general relativistic potentials suggests placing the disk inner boundary at $R = 6M$ for Schwarzschild spacetime and $R = 1.23M$ for the near-maximal Kerr spacetime.

Relating the observed flux to the fundamental disk structure is substantially more complex in the relativistic case because of the complexities of general relativistic photon propagation. For a given value of the stress \mathcal{W} , energy conservation gives that the total radiative flux from one side of the disk, measured in the locally orbiting frame, is (Novikov & Thorne 1973)

$$F(R) = \frac{3\mathcal{D}}{4\mathcal{C}}\Omega\mathcal{W}. \quad (24)$$

Suppose that the corresponding energy-integrated (but angle-dependent) intensity is $I_e(R, \theta)$, where θ is measured from the normal to the disk plane (in the locally orbiting frame of

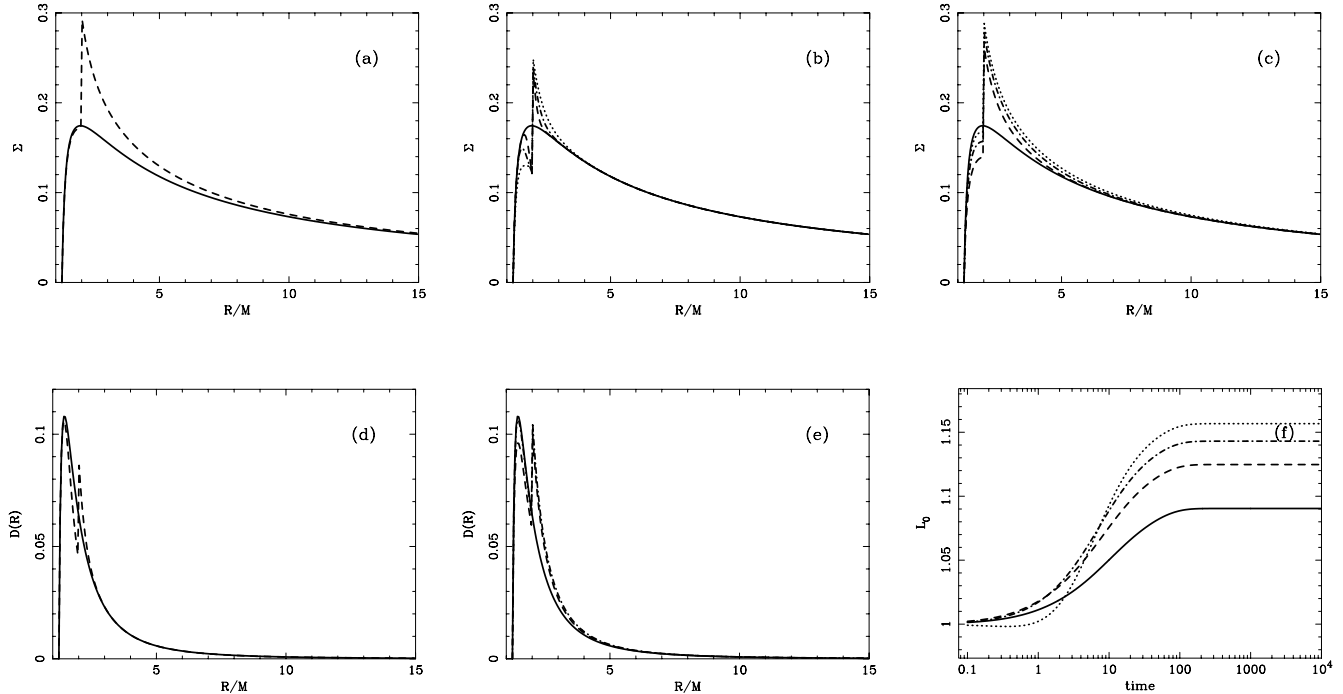


FIG. 4.—Evolution of disk in Kerr spacetime for torque at $R/M = 2$ and spin parameter $a = 0.998$. (a) Surface density profile in untorqued steady state (solid line), as well as the approach to steady state torqued profile (dashed line: $t = 10,000$). (b) Early stages in the evolution of the surface density profile with the solid line being the untorqued steady state profile (solid line: $t = 0$) and the other profiles matching the times and line styles for Fig. 3b. (c) Untorqued steady state profile (solid line), as well as the late-time evolution of the torqued profile (dashed line: $t = 25$, dot-dashed line: $t = 80$, dotted line: $t = 253$). (d) Early evolution of the dissipation profile in addition to the untorqued steady state (solid line) for the same times and line styles as Fig. 3d. (e) Late-stage evolution of the dissipation function with times and line styles compatible with those of Fig. 3e. (f) Luminosity observed at the same angles as in the Schwarzschild case (10° , solid line; 30° , dashed line; 60° , dot-dashed line; 80° , dotted line). The lack of a drop in the observed luminosity comes from the presence of the external torque nearer to the inner boundary in the radial coordinate than in the Schwarzschild case.

reference). Following Cunningham (1975), an observer at infinity will see an integrated luminosity,

$$L_0 = \int \int 2\pi I_e \Upsilon g^3 (g^* - g^{*2})^{-1/2} dg^* d(\pi R^2), \quad (25)$$

where we have followed the notation of Cunningham (1975) with the exception of Υ . Here Υ is the relativistic transfer function that results from ray-tracing null geodesics through the Kerr metric from the disk to the observer. We have used the code of R. Speith (Speith et al. 1995) to compute Υ and hence perform this integral in order to examine how the observed luminosity changes through the torquing event.

These calculations uncover a fundamental difference between the Newtonian and relativistic cases. In the relativistic case, the observed changes in luminosity are a function of the inclination angle of the observer because of the effects of light bending and relativistic beaming of the disk emission. Figures 3f and 4f show the temporal behavior of the observed flux (normalized to the flux for the untorqued disk) for various observing angles for our Schwarzschild and near-extremal Kerr cases, respectively. The final fractional increase in observed flux depends on the beaming pattern of the torque-energized region of the disk compared with that of the untorqued disk. For our Schwarzschild case (Fig. 3f), one can see that the final fractional increase in observed luminosity depends very weakly on the observing angle, implying that the untorqued disk and the torque-energized region of the torqued disk have very similar beaming patterns. There is, however, a much more pronounced temporary decrease in observed flux at higher inclinations due to the temporary dimming of the (more highly beamed) inner regions of the disk. For our Kerr case, the

final fractional increase in observed luminosity increases by almost a factor of 2 as one moves from almost face-on to almost edge-on disks, implying that the torque-energized region of the disk is significantly more beamed than the untorqued disk. A temporary decrease is only observed for the most edge-on cases, again because of a temporary dimming of the innermost regions of the disk.

These features are all symptomatic of the fact that our black hole torques our accretion disk and deposits energy and angular momentum in the disk. This extra source of energy that is dumped into the disk and that tends to affect the disk outward of the external torque location constitutes the starting point for the analysis of § 4, where we attempt to explain the “deep minimum state” as the result of just such a sporadic torquing event.

4. CAN WE INTERPRET THE “DEEP MINIMUM STATE” OF MCG –6-30-15 AS A SPORADIC TORQUING EVENT?

In addition to exploring the general characteristics of sporadically torqued disks, a central motivation for this study is the recent *XMM-Newton* observations of the Seyfert galaxy MCG –6-30-15. In particular, we would like to explore whether the enigmatic “deep minimum state” of this AGN could correspond to a sporadic torquing event, possibly induced by the formation of a temporary magnetic connection between the inner accretion disk and either the plunging region of the disk or the rotating event horizon. There are two defining characteristics of the deep minimum state that must be reproduced by any successful model, the extremely broadened X-ray reflection features (implying a very centrally concentrated X-ray irradiation pattern) and the factor of 2–3 drop in the observed X-ray continuum flux.

A major uncertainty in relating disk models to X-ray observations is always the relation between the dissipation within the disk (predicted by the models) and the emission of the observed X-rays. If we suppose that a local disk corona radiates a fixed fraction of the underlying dissipation into the X-ray band, the results of this paper quickly lead to a contradiction between the sporadically torqued disk model and the observations. While the model does predict a temporary dip in observed luminosity for some observer inclinations (that one might be tempted to identify with the continuum drop in the deep minimum), this dip is due to a dimming of the innermost regions of the accretion flow as a result of the damming of the mass flux. This is precisely the part of the flow that we wish to be enhanced in order to explain the simultaneous broadening of the X-ray reflection features.

Within the (standard) accretion disk corona framework, the relation between the dissipation within the disk and the emission of the observed X-rays depends on the reprocessing of disk photons by the corona. We suggest that this relation changes when the system departs from steady state as the sporadic torque engages, and we use this, in the next section, to model the deep minimum spectrum.

4.1. *Quenching the X-Ray Corona with Returning Radiation*

The assumption that the X-ray emission from the disk corona locally tracks the dissipation in the underlying accretion disk is clearly an oversimplification. For example, Hawley & Krolik (2001) have used high-resolution pseudo-Newtonian simulations to show that there is a rather extended transition (occurring near but slightly outside the radius of marginal stability) from the pure MHD turbulent region characterizing the bulk of the disk to the more laminar flow present in the plunging region. Since the heating of the corona is almost certainly due to reconnection and MHD wave heating from the underlying disk, the fraction of the dissipated energy transported to the corona will certainly change within this transition region, leading to a violation of the simple assumption employed in our toy models. A time-variable magnetic torque of the kind we envision in this paper might alter the MHD and thermodynamic properties of the gas, and such a scenario might not be compatible with the one we describe in the thin-disk approximation. In other words, we can imagine that the external torque changes both the radiative efficiency of the gas, as well as local MHD properties, thereby invalidating the treatment of the magnetorotational instability as a local kinematic viscosity. This fact is most likely more important for thick disks, where the degrees of freedom are greater. Global disk simulations focusing on the formation and properties of the corona are required to address this issue and, hence, are beyond the scope of this paper.

We do, however, note an important and mostly neglected physical effect that could substantially change the structure of a disk corona in a strongly torqued disk—Compton cooling by flux emitted elsewhere in the accretion disk and, in particular, by “returning radiation.” Consider a geometrically thin accretion disk around a near-extremal Kerr black hole, and suppose that it possesses a disk-hugging X-ray corona energized from the underlying disk. Now suppose that the central regions of the disk are subjected to a significant torquing event. As shown above, the work done by the torque is rapidly radiated from the accretion disk in a very centrally concentrated manner. The torque-induced emission will be a combination of both thermal optical/UV radiation and hard X-ray emission produced by the corona associated with the torque-energized regions of the disk. Now, some fraction of the torque-induced emission will strike the disk at

larger radii—this will be particularly prevalent if the disk is flared or warped but will occur even in flat disks because of relativistic light-bending effects (i.e., returning radiation; Cunningham 1973). This extra irradiation will enhance the Compton cooling of the corona at these larger radii. At the very least, the additional cooling will lead to a decrease in the Compton amplification factor of the corona and a steepening of the coronal emission. One could envisage a situation, however, in which the Compton cooling becomes so extreme that the corona completely collapses and local EUV/X-ray emission ceases.

Some essential aspects of this scenario can be captured in a simple model based on energy conservation, following Haardt & Maraschi (1991, 1993). Consider the X-ray-emitting corona above a unit area patch of the disk at a radius r . If a fraction f of the energy dissipated in the underlying disk goes into heating the corona, the heating rate is

$$\mathcal{H}(r) = fD(r). \quad (26)$$

By definition, the (Compton) cooling rate of the corona is $(A - 1)F_s$, where A is the Compton amplification factor and F_s is the soft photon flux passing through the corona, which will act as seed photons for the inverse Compton scattering process that generates the X-rays. Equating heating and cooling gives

$$fD(r) = (A - 1)F_s. \quad (27)$$

We now determine F_s by examining energy conservation of the colder disk underlying the corona. There are three contributions to that that we must consider. First, the portion of the internal dissipation within the disk that does *not* get transported into the disk will become thermalized in the cold disk and contribute an amount $(1 - f)D(r)$ to the disk heating. Second, some fraction of the locally generated coronal flux $\xi_1 fD(r)$ will impinge on the disk and be reprocessed into soft flux. The parameter ξ_1 encapsulates possible anisotropies in the coronal flux and the albedo of the disk but will typically be of the order of $\xi_1 \sim 0.2 - 0.5$. Finally, as noted above, irradiation of our coronal patch from other radii in the disk will contribute to the soft flux and hence the Compton cooling. This will cool the corona because of both the direct action of the irradiating soft flux and the reprocessing/thermalization of the soft and hard irradiating flux. Suppose that the nonlocal irradiating flux is $\mathcal{R}(r)$ times the locally produced flux. The corresponding soft flux contributing to the Compton cooling will be $\xi_2 \mathcal{R}D(r)$, where $\xi_2 \lesssim 1$ parameterizes the fraction of this nonlocal emission that ends up as soft flux. Hence, the total soft flux at a particular location in the disk will be

$$F_s = \xi_1 fD(r) + \xi_2 \mathcal{R}(r)D(r) + (1 - f)D(r). \quad (28)$$

Solving for A , we get

$$A = 1 + \frac{f}{\xi_2 \mathcal{R}(r) + 1 - f(1 - \xi_1)}. \quad (29)$$

Of course, within this simple model the total energy dissipated within the corona is a fixed fraction of the underlying dissipation irrespective of the (cooling) soft flux. However, the amplification factor is significantly reduced by returning radiation if $\mathcal{R}(r) \gtrsim \xi_2^{-1}[1 - f(1 - \xi_1)]$, which, for canonical values of $f = 1$ and $\xi_1 = \xi_2 = 0.5$, corresponds to $\mathcal{R}(r) \gtrsim 1$. The resulting coronal spectrum from the affected regions of the disk would be expected

to steepen significantly, possibly placing a large fraction of the emission into the unobservable EUV band.

For a flat disk at large radii subjected to returning radiation, we have $\mathcal{R}(r) = R_0(a) + \Delta\eta R_\infty(a)$, where $\Delta\eta$ is the enhancement in the efficiency of the disk due to the inner torque and $R_\infty(a)$ and $R_0(a)$ are dimensionless functions of the black hole spin parameter given by the fitting formulae of Agol & Krolik (2000). For a near-extremal Kerr black hole ($a = 0.998$), we have $R_0 \approx 0.2$ and $R_\infty \approx 1$. Thus, we can see that even in the absence of disk flaring or warping, returning radiation alone could significantly depress coronal X-ray activity at large radii if

$$\Delta\eta \gtrsim \frac{1 - f(1 - \xi_1)}{\xi_2} - 0.2. \quad (30)$$

Thus, although there is some dependence on the properties (e.g., isotropy and patchiness) of the corona and the ability of the disk to reprocess and thermalize any incoming flux, the corona will be depressed if the disk is in a “spin-dominated” state ($\Delta\eta \gtrsim 1$), i.e., a state in which the disk is shining via the release of black hole spin energy rather than gravitational potential energy.

4.2. A Proposed Scenario for the MCG –6-30-15 Deep Minimum State

Let us now return to MCG –6-30-15 and the sporadic external torque model for its deep minimum state. We suppose that the normal state of this system is that of a standard untorqued accretion disk that might well be described by the standard accretion models of Novikov & Thorne (1973) and Page & Thorne (1974). We then suppose that some shift in magnetic configuration caused the accretion disk to become magnetically torqued by either the plunging region or the rotating black hole itself. We hypothesize that this event signals the onset of a deep minimum state.

On timescales shorter than the viscous timescale of the inner disk ($t_{\text{visc}} \sim 1$ hr), we expect this torquing event to lead to a damping of the accretion flow and a true dimming of the disk interior to the location where the connection has occurred. However, on longer timescales, the disk will tend to the new torqued steady state (provided that the torque is sufficiently long-lived).

If the magnetic torquing occurs in the very centermost regions of the disk (which is likely in all of the scenarios that we are envisaging), the torqued steady state will possess a much more centrally concentrated dissipation pattern. As described above, some fraction of this central flux will strike the disk farther out (the returning radiation phenomenon) and possibly lead to a Compton suppression of the X-ray-emitting corona there. Only the central portions of the X-ray-emitting corona that are being vigorously energized will contribute significantly to the observed X-ray flux.

It is simple to see that the *overall X-ray luminosity* escaping the system is unlikely to drop and will probably rise within this scenario—the nonlocal cooling is only important for $\Delta\eta > 1$, in which case the part of the disk directly energized by the torque will produce coronal luminosity in excess of $f\dot{M}c^2$. Even accounting for the fact that half of this may strike the disk and be reprocessed into soft flux, the *overall X-ray luminosity* of the torqued disk will inevitably exceed that of the untorqued disk ($0.3\dot{M}c^2$). However, the highly centrally concentrated nature of the torqued emission, coupled with the suppression of the X-ray emission at larger radii, means that this X-ray luminosity is highly beamed into the plane of the disk (see Fig. 10 of Dabrowski et al. 1997), and the *observed X-ray flux* for an observer with an in-

clination of 30° can readily drop. In other words, the observed coronal activity is suppressed by cooling from a powerful photon source that goes largely unobserved because of beaming effects.

5. DISCUSSION AND CONCLUSIONS

Both nonrelativistic and fully relativistic MHD simulations of black hole accretion suggest the ubiquity of weak torques across the radius of marginal stability (Hawley & Krolik 2001, 2002; De Villiers et al. 2003; Gammie et al. 2004). However, it is still far from clear whether these torques can ever achieve the strength required to allow a decline of the overall mass-energy of the black hole, due to spin-down of the hole, which is a requirement for the kind of spin-dominated accretion disks that we have been discussing within the context of MCG –6-30-15. Significantly more simulation work is needed to address this question.

If one makes the assumption that such strongly torqued disks are possible, they provide a plausible and theoretically attractive explanation for the extremely broadened X-ray reflection features seen in the deep minimum state of MCG –6-30-15 (Wilms et al. 2001; Reynolds et al. 2004), as well as the Galactic black hole binary XTE J1650–500 (Miller et al. 2002). Given this hypothesis, we can ask whether the onset of the deep minimum state corresponds to the occurrence of a strong torquing event.

We address this question through analytic and semianalytic time-dependent toy models of torqued accretion. Using these models, we have shown that the simple model of a sporadically torqued disk *fails* to explain the phenomenology of the deep minimum state transition. However, it would be premature to dismiss torqued-disk models on the basis of this failure. In particular, the real culprit may be the assumption that the local X-ray emission is a fixed fraction of the dissipation in the underlying disk. We discuss a particular scenario in which all but the innermost X-ray-emitting corona is quenched by returning radiation when the torque is engaged. Other possibilities include changes in the structure of the MHD turbulence as a result of the strong torquing event that, in turn, could readily change the fraction of the dissipated energy that is transported into the corona.

An alternative paradigm is the gravitational light-bending model of Fabian & Vaughan (2003) and Miniutti & Fabian (2004). Here the primary X-ray source is located on the black hole spin axis. A transition into the deep minimum state corresponds to a migration of the X-ray source down to $2\text{--}3 GM/c^2$, with the light bending producing both an enhancement in the central illumination of the accretion disk and a dimming of the observed X-ray continuum flux. While the physical nature of the axial X-ray source remains unclear, it is an appealing aspect of this model that it reproduces the long-term temporal behavior of the iron line strength (Miniutti & Fabian 2004).

As is often the case, it is uncertainty in the geometry of the primary X-ray source that prevents us from distinguishing between the torqued-disk and light-bending models. The most promising observational approach is to search for a reverberation delay between short-timescale flickering in the X-ray continuum and the corresponding response in the X-ray reflection signatures. If measurements of this time delay demonstrate that the X-ray source in the deep minimum is indeed $2\text{--}3 GM/c^2$ [corresponding to $10\text{--}15 (M/10^6 M_\odot) \text{ lt-s}$] above the central disk plane, strong light bending must occur and the need for a torqued disk is removed. Measurements of this time delay will constrain the X-ray source geometry and allow the degeneracy between these two models to be resolved.

We thank Andy Fabian, Ted Jacobson, Julian Krolik, Barry McKernan, Cole Miller, Eve Ostriker, Brian Punsly, Joern Wilms, and Andy Young for stimulating conversations while this work was being performed and Laura Brenneman, whose code pro-

vided the basis for the generation of Figures 3*f* and 4*f*. We also thank the anonymous referee for useful comments that led to the improvement of this paper. We gratefully acknowledge support from the National Science Foundation under grant AST 02-05990.

REFERENCES

- Agol, E., & Krolik, J. H. 2000, *ApJ*, 528, 161
 Blandford, R. D., & Znajek, R. L. 1977, *MNRAS*, 179, 433
 Cunningham, C. T. 1973, Ph.D. thesis, Univ. Washington
 ———. 1975, *ApJ*, 202, 788
 Dabrowski, Y., Fabian, A. C., Iwasawa, K., Lasenby, A. N., & Reynolds, C. S. 1997, *MNRAS*, 288, L11
 De Villiers, J. P., Hawley, J. F., & Krolik, J. H. 2003, *ApJ*, 599, 1238
 Eardley, D., & Lightman, A. 1975, *ApJ*, 200, 187
 Fabian, A. C., Rees, M. J., Stella, L., & White, N. E. 1989, *MNRAS*, 238, 729
 Fabian, A. C., & Vaughan, S. 2003, *MNRAS*, 340, L28
 Fabian, A. C., et al. 2000, *PASP*, 112, 1145
 Ford, R. J., et al. 1994, *ApJ*, 435, L27
 Gammie, C. F. 1999, *ApJ*, 522, L57
 Gammie, C. F., Shapiro, S. L., & McKinney, J. C. 2004, *ApJ*, 602, 312
 Greenhill, L. J., Jiang, D. R., Moran, J. M., Reid, M. J., Lo, K. Y., & Claussen, M. J. 1995, *ApJ*, 440, 619
 Haardt, F., & Maraschi, L. 1991, *ApJ*, 380, L51
 ———. 1993, *ApJ*, 413, 507
 Harms, H. C., et al. 1994, *ApJ*, 435, L35
 ———. 2001, *ApJ*, 548, 348
 ———. 2002, *ApJ*, 566, 164
 Hirose, S., Krolik, J. H., De Villiers, J.-P., & Hawley, J. F. 2004, *ApJ*, 606, 1083
 Iwasawa, K., et al. 1996, *MNRAS*, 282, 1038
 Krolik, J. H. 1999a, *ApJ*, 515, L73
 ———. 1999b, *Active Galactic Nuclei* (Princeton: Princeton Univ. Press)
 Li, L.-X. 2002, *ApJ*, 567, 463
 Miller, J. M., et al. 2002, *BAAS*, 34, 1206
 Miniutti, G., & Fabian, A. C. 2004, *MNRAS*, 349, 1435
 Miyoshi, M., Moran, J., Herrnstein, J., Greenhill, L., Nakai, N., Diamond, P., & Inoue, M. 1995, *Nature*, 373, 127
 Novikov, I., & Thorne, K. S. 1973, in *Black Holes*, ed. C. DeWitt & B. DeWitt (New York: Gordon & Breach), 345
 Page, D. N., & Thorne, K. S. 1974, *ApJ*, 191, 499
 Press, W. H., Teukolsky, S. A., Vetterling, W. T., & Flannery, B. P. 1992, *Numerical Recipes in C: The Art of Scientific Computing* (Cambridge: Cambridge Univ. Press)
 Pringle, J. E. 1981, *ARA&A*, 19, 137
 Reynolds, C. S., & Nowak, M. A. 2003, *Phys. Rep.*, 377, 389
 Reynolds, C. S., Wilms, J., Begelman, M. C., Staubert, R., & Kendziorra, E. 2004, *MNRAS*, 349, 1153
 Shakura, N. I., & Sunyaev, R. A. 1973, *A&A*, 24, 337
 Speith, R., Riffert, H., & Ruder, H. 1995, *Comput. Phys. Commun.*, 88, 109
 Tanaka, Y., et al. 1995, *Nature*, 375, 659
 Williams, R. K. 2004, *ApJ*, 611, 952
 Wilms, J., Reynolds, C. S., Begelman, M. C., Reeves, J., Molendi, S., Staubert, R., & Kendziorra, E. 2001, *MNRAS*, 328, L27